

Is there room for highly magnetized pulsar wind nebulae among those non-detected at TeV?

J. Martin¹, D. F. Torres^{1,2}, A. Cillis³ & E. de Oña Wilhelmi¹

¹*Institute of Space Sciences (IEEC-CSIC), Campus UAB, Torre C5, 2a planta, 08193 Barcelona, Spain*

²*Institució Catalana de Recerca i Estudis Avançats (ICREA) Barcelona, Spain*

³*Instituto de Astronomía y Física del Espacio, Casilla de Correo 67 - Suc. 28 (C1428ZAA), Buenos Aires, Argentina*

ABSTRACT

We make a time-dependent characterization of pulsar wind nebulae (PWNe) surrounding some of the highest spin-down pulsars that have not yet been detected at TeV. Our aim is assessing their possible level of magnetization. We analyze the nebulae driven by J2022+3842 in G76.9+1.0, J0540-6919 in N158A (the Crab twin), J1400-6325 in G310.6-1.6, and J1124-5916 in G292.0+0.18, none of which have been found at TeV energies. For comparison we refer to published models of G54.1+0.3, the Crab nebula, and develop a model for N157B in the Large Magellanic Cloud (LMC). We conclude that further observations of N158A could lead to its detection at VHE. According to our model, a FIR energy density of 5 eV cm^{-3} could already lead to a detection in H.E.S.S. (assuming no other IC target field) within 50 hours of exposure and just the CMB inverse Compton contribution would produce VHE photons at the CTA sensitivity. We also propose models for G76.9+1.0, G310.6-1.6 and G292.0+1.8 which suggest their TeV detection in a moderate exposure for the latter two with the current generation of Cherenkov telescopes. We analyze the possibility that these PWNe are highly magnetized, where the low number of particles explains the residual detection in X-rays and their lack of detection at TeV energies.

Key words: pulsar wind nebulae

1 INTRODUCTION

The spectral energy distribution (SED) of the pulsar wind nebulae (PWNe) of the highest spin-down powered pulsars is diverse. In particular, luminous pulsars such as Crab ($L_{sd} = 4.5 \times 10^{38} \text{ erg s}^{-1}$) and the Large Magellanic Cloud (LMC) J0537-6910 in N157B ($L_{sd} = 4.9 \times 10^{38} \text{ erg s}^{-1}$) are TeV detected, as are others with spin-down power in the order of several $10^{37} \text{ erg s}^{-1}$. However, several PWNe with pulsars similarly luminous, are not. Why? Do they have significantly different interstellar environment, injection, or nebular magnetization?

The X-ray luminosity efficiency of these high-spin down pulsars also presents a large range. A notable case is G76.9+1.0 for which the X-ray efficiency is $L_X/L(t) \sim 2.4 \times 10^{-4} D_{10}^2$, where D_{10}^2 is the distance in units of 10 kpc (Arzoumanian et al. 2011).¹ This and similar cases are

challenging for PWNe spectral models since they imply an inefficient acceleration of high energy electrons in order to fit the X-ray luminosity. For these cases, Arzoumanian et al. (2008) suggested that the pulsar wind has a high magnetization factor, arguing that because particle-dominated winds are necessary for efficient conversion of wind to synchrotron power, PWNe with high magnetization would lead to dim X-ray PWNe. Thus, high- η (high magnetic fraction) models point to an interesting alternative for the interpretation of PWNe, which, despite their high spin-down, lack TeV emission and have weak X-ray counterparts. These PWNe would be different to TeV detected ones. Except CTA 1, for which the magnetization reaches almost to equipartition, all TeV-PWNe with characteristic ages of 10 kyr or less can be described with an spectral model with low η , and are thus strongly particle dominated (Torres et al. 2014).

An interesting case is that of G292.0+0.18, for which the central powering pulsar, J1124-5916, has essentially the same P , \dot{P} (up to three significant decimal places) than J1930+1852, which powers G54.1+0.3. The distance for both nebulae is also similar (~ 6 kpc). Whereas the latter is a TeV source, and modeled as particle dominated PWN (e.g.,

¹ The spin-down of the pulsar in G76.9+1.0 has been recently re-assessed due to a new measurement of the period (see the discussion below). While it is now lower than earlier claimed, it still qualifies as one the most energetic pulsars we know.

Tanaka & Takahara 2011, Torres et al. 2014), the former is not (at least at the level in which it has been covered in the Galactic Plane observations by H.E.S.S. (Carrigan et al. 2013)). With the same spin-down power and located at a similar Galactic distance, it seems that the flux at TeV energies depends on other factors such the environment (the FIR density, for instance) or the nebula magnetization. Is then G292.0+0.18 simply like G54.1+0.3 but subject to a stronger magnetization?

Tanaka & Takahara (2013) have also analyzed several PWNe which have been undetected at TeV.² However, they assumed a fixed low magnetization (3×10^{-3}) compatible with usual particle dominated nebulae that have been detected at TeV to describe them. In this work, we explore the phase space of PWNe models also in magnetization, in order to distinguish whether there is preference for the existence of highly magnetized nebulae (or at least, for nebula with magnetization close to equipartition) among those not yet seen at TeV.

2 SPECTRAL MODEL

The code we use solves the time-dependent diffusion-loss equation for the electrons in the PWN, and includes the energy losses due to synchrotron, IC, adiabatic and Bremsstrahlung processes, and escape due to Bohm diffusion (see Martin et al. 2012; Torres et al. 2013a,b for details). We shall refer with $Q(\gamma, t)$ to the injection function, generally assumed as a broken power law with γ_b being the energy of the break (in Lorentz factor units) and α_l and α_h , the low and high energy indices respectively. The normalization of the injection is computed using the spin-down luminosity of the pulsar $L(t)$ and the magnetic fraction η

$$(1 - \eta)L(t) = \int_{\gamma_{min}}^{\gamma_{max}} \gamma m_e c^2 Q(\gamma, t) d\gamma. \quad (1)$$

The evolution of the magnetic field is described by (e.g., Pacini & Salvati 1973)

$$B(t) = \frac{1}{R_{PWN}^2} \left[6\eta \int_0^t L(t') R_{PWN}(t') dt' \right]^{1/2}. \quad (2)$$

The spin-down power evolution is deduced assuming that the pulsar has the same behavior as a spinning magnetic dipole with braking index n .

We refer with $\tau_0 = 2\tau_c/(n-1) - t_{age}$ to the initial spin-down age, and with τ_c to the characteristic age of the pulsar. The maximum energy of the particles is calculated by the requirement that their Larmor radius is smaller than the termination shock radius. The radius of the nebula is computed assuming free expansion of the shell in the interior of the supernova remnant (SNR). If we consider that the spin-down luminosity of the pulsar is constant, it evolves as (van der Swaluw et al. 2001) $R_{PWN}(t) =$

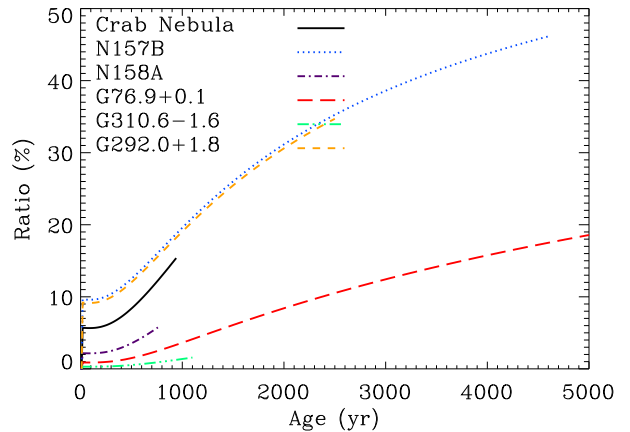


Figure 1. Ratio of the PWN radii resulting from the analytical and numerical models as commented in the text, for some of the nebulae studied.

$0.839 (L_0 t / E_0)^{1/5} V_0 t$, with $V_0 = \sqrt{10E_0/3M_{ej}}$. We shall refer to this radius as $R_{analytical}$. This value is obtained by assuming that all the mechanical energy of the explosion with energy E_0 is transformed into kinetic energy. M_{ej} is the ejected mass in the explosion. L_0 is the initial spin-down luminosity of the PSR. In some of the PWNe that we study in this work, the spin-down power of the pulsar is very high and its variation in time cannot be neglected. For this reason, we solve numerically the energy balance equation

$$\frac{d}{dt}(4\pi R_{PWN}^3 P) = L(t) - 4\pi R_{PWN}^2(t) P(t) \left(\frac{dR_{PWN}}{dt} \right) \quad (3)$$

assuming that the pressure $P(t)$ of the PWN at the contact discontinuity with the expanding ejecta is given by (equation A7 in van der Swaluw et al. 2001)

$$P(t) = \frac{3}{25} \rho_{ej}(t) \left(\frac{R_{PWN}(t)}{t} \right)^2, \quad (4)$$

which depends on the density of the SNR ejecta ρ_{ej} . Fig. 1 shows the fractional deviation between the radii, i.e., $(R_{analytical} - R_{numerical})/R_{analytical} \times 100$, using the parameters obtained of Table 1. We observe that the difference in radius goes from $\sim 2\%$ (for G310.6-1.6) to $\sim 46\%$ (for N157B), being larger for when the spin-down luminosity is constant. Taking into account that the magnetic field depends on the radius as $B \sim R_{PWN}^{-3/2}$, this changes the magnetic field of the nebula, and consequently, its synchrotron flux. Another affected parameter in the fits is the ejected mass of the progenitor star, because the velocity of the ejecta behaves with the mass as $V_0 \sim M_{ej}^{-1/2}$. This means that with the numerical solution, the ejected mass needed to reach a given radius R_{PWN} has to be smaller, due to the decreasing spin-down power in time. Regarding the SSC radiation, we assume that the synchrotron ball generating the multi-frequency radiation from each of the PWN has the same radius at all energies, and is equal to the radius of the PWN itself.

In order to fit the spectra, we fix from observations as many parameters as possible. Generally, we fix the period (P), period derivative (\dot{P}), braking index (n), age of the sys-

² For differences between their model and ours see the discussion in Martin et al. (2012) and Torres et al. (2014). Their magnetic field evolution does not consider losses in magnetic energy due to expansion, and thus their magnetization values are lower than ours typically by a factor 2-3.

tem (t_{age}), initial spin-down age (τ_0), spin-down luminosity ($L(t)$), distance (d), radius of the PWN (R_{PWN}), minimum energy at injection (γ_{min}), and FIR and NIR temperatures (T_{FIR} , T_{NIR}). The rest of parameters are fitted or derived from the others.

3 LARGE MAGELLANIC CLOUD'S N157B & N158A

N157B is located in the LMC and it was the first extragalactic PWN detected in gamma rays (Abramowski et al. 2012). Its pulsar, PSR J0537-6910, has a spin-down power of 4.9×10^{38} erg s $^{-1}$ (Manchester et al. 2005). Lazendic et al. (2000) did radio observations of this PWN using the Australia Telescope Compact Array (ATCA), obtaining a spectral index of -0.19 . Micelotta et al. (2009) did infrared observations using the *Spitzer* telescope but reported no infrared counterpart (no bright SNR). Studying the gas and dust properties of the vicinity, they deduced that the mass of the progenitor star should not be higher than $25M_{\odot}$. In X-rays, N157B was observed with *ASCA* and *ROSAT* (Wang & Gotthelf 1998), and Wang et al. (2001) detected the PWN with *Chandra*. Chen et al. (2006) analyzed the spectrum of N157B and the pulsar PSR J0537-6910 in X-rays. The spectrum of the entire remnant is fitted with a dominant non-thermal component (a power-law with a spectral index of 2.29 and an unabsorbed flux of 1.4×10^{-11} erg s $^{-1}$ cm $^{-2}$) and a thermal component (a NEI model with a temperature of 0.72 keV and an unabsorbed flux of 7×10^{-12} erg s $^{-1}$ cm $^{-2}$).

In our study, we use the estimated distance of 48 kpc, see Abramowski et al. (2012). There are two gas bubbles in the vicinity of N157B which contribute to the far-infrared (FIR) photon fields: 30 Doradus complex and the OB association LH99. From the infrared observations done by Indebetouw et al. (2009), Abramowski et al. (2012) modelled the infrared emission as a black body with energy density of 8.9 eV cm $^{-3}$ and a temperature of 88 K for the LH99 association, and 2.7 eV cm $^{-3}$ and 80 K for 30 Doradus. They consider these values as an upper limit since the unprojected distance between these objects is unknown.

Figure 2 (left panel) shows the fit we obtain for N157B. We assume the radius for the PWN given by Lazendic et al. (2000), i.e., 10.6 pc for a distance of 48 kpc. The PWN shell is not very well defined and some small contribution of the SNR could be included. In this first model, we assumed an age of 4600 yr, which is consistent with the Sedov age of the SNR given by Wang & Gotthelf (1998) (~ 5 kyr) and an ejected mass of $20M_{\odot}$, corresponding to the lower limit in the ejected mass given by Chen et al. (2006). The electron injection has a low (high) energy index of 1.5 (2.75) and the energy break is located at $\gamma = 10^6$ (~ 511 GeV). From the synchrotron part of the spectrum, we inferred a magnetic field of 13 μ G and a magnetic fraction of 0.006. The energy density of the target photon fields, enhanced due to the near presence of LH99 and 30 Doradus, results in our fits much below the upper limits given by Abramowski et al. (2012), i.e., 0.7 and 0.3 eV cm $^{-3}$, respectively.

If instead we assume the energy densities given by Abramowski et al. (2012), we need to consider a lower age of 2.5 kyr to fit the TeV data. Considering the lower limit on the ejected mass given by Chen et al. (2006), then the

radius decreases until 3.7 pc. Regarding the synchrotron spectrum, the magnetic field reaches 35 μ G and $\eta=0.01$. The intrinsic energy break changes to $\gamma_b = 2 \times 10^5$ (~ 102 GeV) and the injection slopes change slightly ($\alpha_l=1.5$, $\alpha_h=2.6$). The value obtained for the radius in the latter model is only $\sim 50\%$ higher than the radius observed in X-rays. This difference is small in comparison with other cases. For example, for the Crab nebula, we see that the radius in the radio band is ~ 2 pc and in X-rays ~ 0.6 pc. As the shell is not well defined, the radius measured by Lazendic et al. (2000) could include parts of the remnant, but the relation between the PWN radius in X-rays and the radius in the radio band seems to be more similar to the Crab nebula case. van der Swaluw (2004) suggested that N157B PWN could be interacting with the reverse shock of the SNR in a very initial phase, explaining its elongated morphology. In any case, we find that N157B is a luminous particle dominated nebula.

N158A, known as the Crab twin, is also located in the LMC but has not been detected at TeV yet. This PWN is powered by the pulsar PSR B0540-69, which has been observed in radio, infrared, optical and X-ray bands. The period of this pulsar is 50.5 ms (Seward et al. 1984) and the period derivative is 4.7×10^{-13} s s $^{-1}$ (Livinstone et al. 2005). The resulting spin-down luminosity is then 1.5×10^{38} erg s $^{-1}$. The diameter of N158A is 1.4 pc, as obtained from radio observations (Manchester et al. 1993b). The distance to PSR B0540-69 has been estimated as ~ 49 kpc (Seward et al. 1984; Taylor & Cordes 1993; Słowikowska et al. 2007). An age of 760 yr is deduced through measurements of the expansion velocity of the SNR shell in the optical spectral range (Reynolds 1985; Kirshner et al. 1989). There is no observational measurement of the ejected mass in N158A, and we have left this parameter free in our model. The resulting ejected mass in our fits is $25M_{\odot}$. According to Heger et al. (2003), this mass is at the limit for neutron star creation, which can grow with the quantity of helium in the core of the star and the energy of the supernova explosion. In the infrared, Caraveo et al. (1992) did a high-resolution observation of N158A using the European Southern Observatory New Technology Telescope (*ESO-NTT*) and concluded that the progenitor of the SNR could have belonged to the same generation of young stars in 30 Doradus (Caraveo et al. 1992; Kirshner et al. 1989). Williams et al. (2008) did not find evidence of infrared emission from the SNR, but they inferred a mass of $20-25M_{\odot}$ for the progenitor star. PSR B0540-69 is one of the few pulsars with optical pulsations and polarized emission. Its optical spectrum is well fitted by a power-law, but joining it with the X-ray spectrum, a double break is required (Mignani et al. 2012). The braking index for PSR B0540-69 is 2.08 (Kaaret et al. 2001). A high-resolution X-ray observation was done with *Chandra* (Gotthelf & Wang 2000; Kaaret et al. 2001) and there is also a compilation of the observations done with *RXTE*, *Swift* and *INTEGRAL* in the work by Campana et al. (2008). The flux obtained for the PWN is $\sim 8 \times 10^{-11}$ erg s $^{-1}$ cm $^{-2}$. There is no detection of the PWN at VHE.

For N158A, the injection spectrum resulting from our fit is a broken power-law with break at a large energy $\gamma = 3 \times 10^7$ (~ 15.3 TeV) and a low (high) energy spectral index

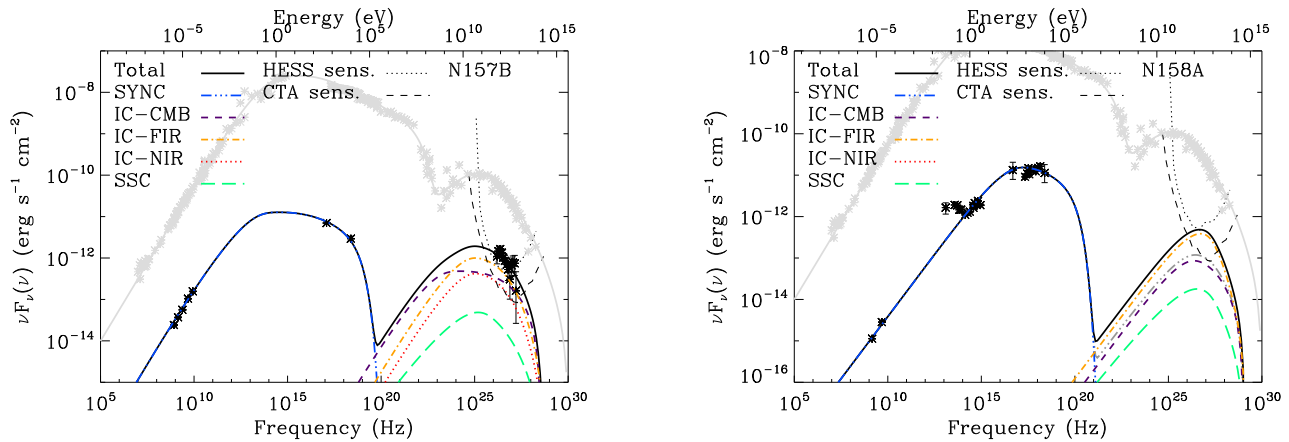


Figure 2. Nebulae in the LMC. Left panel: Spectral fit for the N157B PWN. The fluxes and the fit of the Crab Nebula is overplotted in grey for comparison. We plot also the sensitivity curves of H.E.S.S. and CTA for an exposure time of 50 hours. The data points are obtained from: Lazendic et al. (2000) (radio), Chen et al. (2006) (X-rays), Abramowski et al. (2012) (VHE). Right panel: Spectral fit for the N158A PWN to reach H.E.S.S. (in solid black) and CTA (in triple-dot dashed grey) sensitivities. The data points are obtained from: Manchester et al. (1993b) (radio), Mignani et al. (2012) (infrared & optical), Kaaret et al. (2001), Campana et al. (2008) (X-rays).

of 1.8 (2.6). The synchrotron component is fitted with a magnetic field of $32 \mu\text{G}$. The magnetic fraction in this case is low ($\eta = 0.0007$). Due to the lack of information on the FIR and near-infrared/optical (NIR) fields, we assume a FIR field with a temperature of 80 K and compute the energy density needed for the PWN to be detected by H.E.S.S. or CTA. For H.E.S.S., a minimum energy density of 5 eV cm^{-3} is required to be detected in a 50 hours observation, according to the sensitivity curve used here. For CTA, an energy density of 0.2 eV cm^{-3} would be enough to allow detection, which foresees its identification in case our model is correct. Both models are shown in Fig. 2 (right panel) and their parameters are given in Table 1.

The NIR photon field could also be important depending on the density of nearby stars in the N158A field and could enhance the TeV yield, at the same time reducing the required FIR densities for detection.

We have also investigated highly magnetized models in which the detection of N158A is not possible even with CTA, unless the energy density of the FIR increases up to $\sim 500 \text{ eV cm}^{-3}$ (assuming that there is no NIR contribution). The injection function in such models has an energy break of $\gamma_b = 6 \times 10^7$, and a low (high) spectral index is 1.45 (2.4). Taking into account that the maximum energy at injection is $\gamma_{max} = 1.2 \times 10^8$, a simple power-law model with an index of 1.45 could also be compatible with this fit. Here, we obtain a highly magnetized nebula with a magnetic fraction of 0.9 and an extreme magnetic field of 1.15 mG. But whereas the radio and the infrared data are fitted similarly well to particle dominated models, the predicted X-ray flux of these models is not quite in agreement with data. This fact and the extreme values of the parameters we have just quoted make a high η model unlikely. In equipartition (i.e., $\eta = 0.5$), the radio and X-ray flux surpasses the data flux in a factor ~ 4 . In this latter case, the magnetic field is lower ($B = 858 \mu\text{G}$), but the number of particles is still high to fit the flux.

We conclude that N158A is a particle dominated nebulae that has been undetected because of sensitivity limitations.

4 POWERFUL GALACTIC PULSARS HAVING NEBULAE NON-DETECTED AT TEV YET

4.1 G76.9+1.0

G76.9+1.0 hosts the pulsar PSR J2022+3842. The period and the period derivative of this pulsar was firstly determined by Arzoumanian et al. (2011). They obtained a period of 24 ms and a period derivative of $4.3 \times 10^{-14} \text{ s s}^{-1}$, which implies a spin-down luminosity of $1.2 \times 10^{38} \text{ erg s}^{-1}$. This made PSR J2022+3842 the third pulsar with the highest spin-down known. In later observations with *XMM-Newton*, Arumugasamy et al. (2013) discovered a factor 2 error in the determination of the pulsar period and period derivative. The new period is then 48 ms and the spin-down luminosity reduces to $2.96 \times 10^{37} \text{ erg s}^{-1}$.

The remnant was observed in radio using the Very Large Array telescope (*VLA*) (Landecker et al. 1993). These authors assume a distance of 7 kpc, which implies a size of $18 \times 24 \text{ pc}$. The structure of the SNR is dominated by two lobes oriented in the north-south direction separated by 3 arcmin. The spectral index is 0.62 ± 0.04 . They looked for an infrared counterpart using IRAS data but none was found. Arzoumanian et al. (2011) observed PSR J2022+3842 in X-rays using *Chandra*, obtaining an absorbed X-ray flux (2–10 keV) of $5.3 \times 10^{-13} \text{ erg s}^{-1} \text{ cm}^{-2}$ and detecting a very weak PWN with an absorbed flux of $4 \times 10^{-14} \text{ erg s}^{-1} \text{ cm}^{-2}$. In this case, there is no TeV detection either, and we only have information about the spectrum in X-rays and upper limits in radio using the flux observed for the SNR radio shell.

We adopted an age of 5 kyr, which implies a reasonable ejected mass of $20 M_{\odot}$, also proposed by Arzoumanian et al. (2011). There are no estimations of the age of the remnant and of the ejected mass. Arzoumanian et al. (2011) has established an upper limit on the true age of the pulsar depending on the braking index of $\sim 40 \text{ kyr}$, which is unconstraining.

We use the data simulated by GALPROP (Porter et al. 2006) for the energy densities and temperatures for the FIR and NIR photon fields, essentially, diluted black bodies with

a temperature of 25 K and an energy density of 0.13 eV cm^{-3} for the FIR field, and a temperature of 3200 K and an energy density of 0.33 eV cm^{-3} for the NIR field. As the PWN in X-rays is very diluted, its shell cannot be distinguished. For this reason, to simulate the expansion of the nebula, we assumed a ballistic expansion of the SNR radio shell ($R_{SNR} = V_0 t$) and compute the necessary ejected mass. In this case, we obtain a value of $\sim 20M_\odot$, which implies a radius of $\sim 6.3 \text{ pc}$. We assume a braking index of 3, which implies a reasonable value for the initial period for PSR J2022+3842 of 32 ms.

In model 1, see Table 1, we assume a broken power-law injection with a low-energy (high-energy) spectral index of 1.5 (2.7). The resulting energy break is at $\gamma_b = 10^3$. The magnetic field ($3.5 \mu\text{G}$) is close to the average ISM value. The magnetic fraction is 0.0017. The low value of the injection energy break in this model argues for a possible simple power-law injection. This is assumed in model 2. In this case, the spectral index is 2.6 and the magnetic field is $16.6 \mu\text{G}$, with a magnetic fraction of 0.038. Finally, model 3 explores whether G76.9+1.0 could be a highly magnetic PWN, as speculated previously by Arzoumanian et al. (2008, 2011). The lack of significant observational constraints allows to entertain this possibility, and we show an example with a magnetic field of $85.2 \mu\text{G}$ and a magnetic fraction of $\eta = 0.998$. The injection function in this case is a simple power-law with an spectral index of 2.65. In order to respect the upper limits in radio, we need to impose a minimum energy at injection for particles of $\gamma = 10^4$ ($\sim 5.1 \text{ GeV}$). The IC contribution decreases with respect the other models, as expected due to the lower contribution of spin-down energy to particles and the larger synchrotron field, which maximizes their losses.

The lack of observational data to put sufficient constraints to differentiate the models proposed. In any case, its detection at TeV energies seems unexpected.

4.2 G310.6–1.6

G310.6–1.6 (IGR J14003-6326) was discovered as a soft γ -ray source in a deep mosaic of the Circinus region done by INTEGRAL (Keek et al. 2006). It was also observed in the *Swift* survey of INTEGRAL sources, but without conclusions about its origin (Malizia et al. 2007). With *Chandra* observations, Tomsick et al. (2009) fitted the spectrum (0.3 and 10 keV) of the source with a power-law with a photon index of $\Gamma = 1.82 \pm 0.13$. Renaud et al. (2010) discovered 31.18 ms pulsations using *RXTE*, as well as reported the radio detection of PSR J1400-6325 and its nebula. From the *RXTE* timing analysis, they obtained a period derivative for PSR J1400-6325 of $3.89 \times 10^{-14} \text{ s s}^{-1}$, which implies a spin-down luminosity of $5.1 \times 10^{37} \text{ erg s}^{-1}$ and a characteristic age of 12.7 kyr. There are several estimations of the PWN distance, covering a range between 6 and 10 kpc. We adopt the value of 7 kpc given in Renaud et al. (2010).

Renaud et al. (2010) have studied the spectrum of G310.6–1.6, PSR J1400-6325 and its PWN from 0.8 to 100 keV. The spectrum is highly dominated by the PWN and it is fitted with a broken power-law. The energy break is located at 6 keV and it is probably produced by the synchrotron cooling of the particles. The spectral index for energies lower (higher) than the energy break is 1.90 ± 0.10 (2.59 ± 0.11). The total flux for the PWN at 20–100 keV is

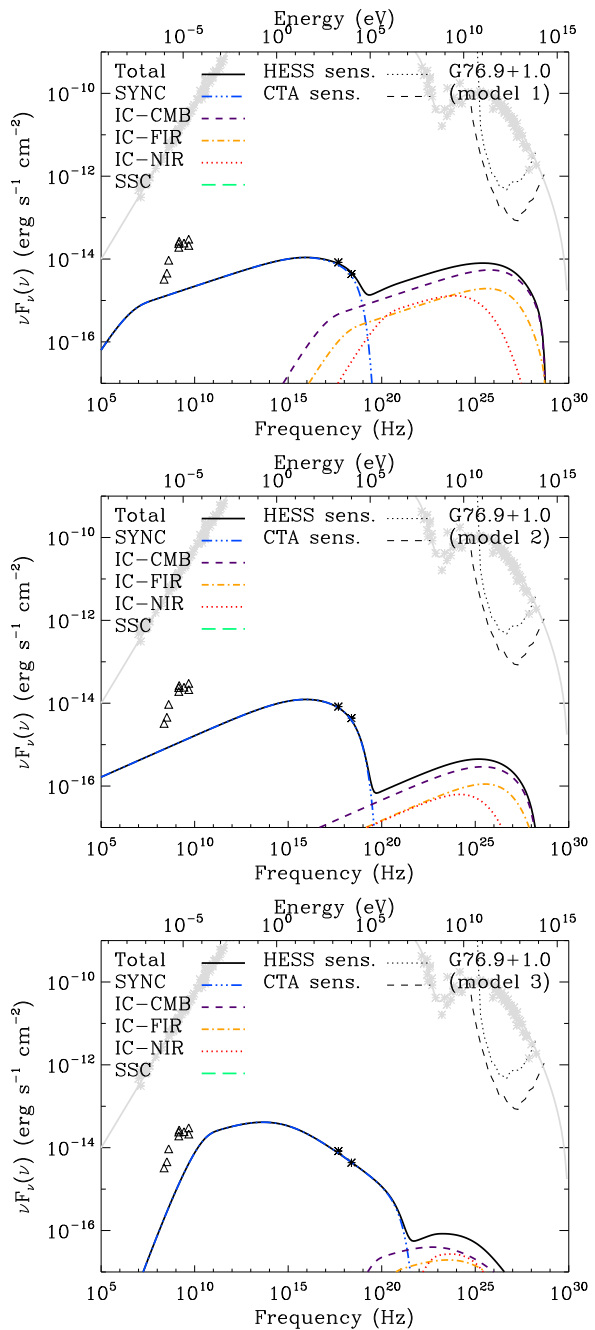


Figure 3. Spectral fits for G76.9+1.0 PWN (models 1 to 3, top to bottom). The triangle data points correspond to the radio flux of the radio shell given in Landecker et al. (1993), here used as upper limits. The X-ray data is obtained from Arzoumanian et al. (2011).

$5.3 \times 10^{-12} \text{ erg cm}^{-2} \text{ s}^{-1}$. The PWN flux in radio frequencies has also been measured, using data from the Molonglo Galactic Plane Survey (Murphy et al. 2007) at 843 MHz, as $217.4 \pm 9.4 \text{ mJy}$, as well as from the Parkes-MIT-NRAO (PMN) survey (Griffith & Wright 1993; Condon et al. 1993) at 4.85 GHz, as $113 \pm 10 \text{ mJy}$. An upper limit of 0.6 mJy at 2.4 GHz is also established by the Parkes telescope (Duncan et al. 1995). At TeV energies, G310.6–1.6 was ob-

served by H.E.S.S. (Chaves et al. 2008), but only an upper limit of 4% of the Crab Nebula was established (Khélifi et al. 2008).

The spectrum of G310.6-1.6 PWN has been previously studied by Tanaka & Takahara (2013). They assumed a magnetic fraction of 0.003, an age of 600 yr and a distance of 7 kpc. For these parameters, they obtained an injection with a low (high) energy spectral index of 1.4 (3.0) with an energy break of $\gamma_b = 3 \times 10^6$ and a magnetic field of $17 \mu\text{G}$. They assumed a 0.3 eV cm^{-3} energy density for the FIR and NIR target photon fields.

In our case, we firstly propose a low magnetized model (model 1), where we assume that the age of the PWN is 1.1 kyr, which is consistent with the upper limit of 1.9 kyr established by Renaud et al. (2010), but older than the one considered in Tanaka & Takahara (2013). This assumption has been done also taking into account the size of the nebula and a reasonable ejected mass of $9 M_\odot$ with a SN energy of 10^{51} erg. Renaud et al. (2010) proposed a subenergetic SN of 5×10^{48} erg setting an ISM density of 0.01 cm^{-3} . This implies an ejected mass of $3M_\odot$ to explain the size of the nebula. This mass is very low for the ejecta of a star that explodes as a SN. We also prefer to consider the canonical value for the SN explosion energy.

The target photon fields are obtained from those computed by GALPROP. The fitted black bodies of these photon fields have a temperature of 25 K and 3300 K and an energy density of 0.63 eV cm^{-3} and 1.62 eV cm^{-3} for FIR and NIR, respectively. The obtained magnetic field is $8.2 \mu\text{G}$ and $\eta=0.0007$. The latter is the same value we find for the particle dominated models of N158A. The value of the magnetic field agrees with the lower limit of $6 \mu\text{G}$ given by Renaud et al. (2010). The intrinsic energy break of the injection in this model is located at $\gamma = 2 \times 10^6$ ($\sim 1 \text{ TeV}$). The injection index at low (high) energies is 1.5 (2.5).

The lack of observational constraints also allows considering an alternative model in which the nebula is a magnetically dominated PWN with $\eta=0.98$, well beyond equipartition. In this case (model 2, see Fig. 4), the energy break moves to higher energies ($\gamma = 6 \times 10^6$ or $\sim 3 \text{ TeV}$) and the magnetic field increases up to $306 \mu\text{G}$. Model 2 explains also well the overall X-ray flux, but fails in reproducing the break at 6 keV.

Future observations of G310.6-1.6 will help to discern definitely between both models. For low- η model, the flux of G310.6-1.6 is a factor \sim over the H.E.S.S. sensitivity flux at 50 h of exposure time. Even with only the CMB contribution, this sensitivity is surpassed by a factor ~ 2 . If the low- η model is right, its detection is expected in a moderate exposure time with the current Cherenkov telescopes.

4.3 G292.0+0.18

As stated in the introduction, the pulsars related with G54.1+0.3 and G292.0+0.18 both have a period of ~ 135 ms, period derivative of $\sim 7.5 \times 10^{13}$, a spin-down power of 1.2×10^{37} erg/s, a characteristic age of ~ 2900 years and a distance of ~ 6 kpc. For both pulsars, the braking index is unknown.

The radius of G292.0+0.18 is based on the SNR size of $8'$ diameter (Gaensler & Wallace 2003), which means a physical radius of 3.5 pc. The distance estimate is based

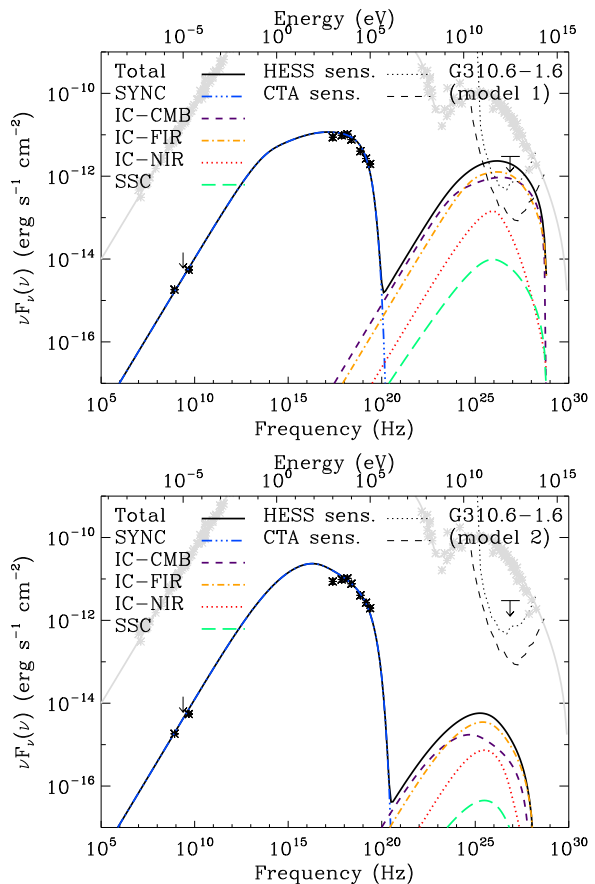


Figure 4. Spectral fits for G310-1.6 PWN (models 1 to 2, top to bottom).

on the HI absorption profile given by Winkler et al. (2009). Based on measurement of the transverse motions of the filaments of the SNR and assuming that the shell is expanding with transverse expansion velocity, Winkler et al. (2009) estimated an age between 3000 and 3400 years, concurring with Gaensler & Wallace (2003). The ejected mass of the SN explosion was estimated as $\sim 6 M_\odot$ (Gaensler & Wallace 2003).

Radio observations for the nebula were obtained from the work of Gaensler & Wallace (2003). The flux of the nebula in X-rays was measured by *Chandra* (Hughes et al. 2001). The photon index of the X-ray spectra, as it is suggested in Hughes et al. (2001), is considered the same as that of the pulsar. At GeV energies, we only have upper limits from Fermi-LAT (Ackermann et al. 2011). Optical and near infrared observations were obtained for the torus of the nebula, by Zharikov et al. (2008) and Zharikov et al. (2013), respectively, but these are not considered in our fits, since do not include the entire system. The background energy densities are unknown. We assume those given by GALPROP, for which the equivalent temperatures and densities of the representing blackbodies are $T_{\text{FIR}}=25 \text{ K}$, $w_{\text{FIR}}=0.42 \text{ eV cm}^{-3}$, and $T_{\text{NIR}}=2800 \text{ K}$, $w_{\text{NIR}}=0.70 \text{ eV cm}^{-3}$.

Fig. 5 shows two models that fit the radio and the X-ray data for this nebula. In both cases the age of the system is 2500 years, and the ejected mass is $9 M_\odot$. In model 1

(see Fig. 5), we consider a low magnetic fraction model with $\eta=0.05$, which is 10 times larger than the magnetic fraction obtained in our model for G54.1+0.3 in Torres et al. (2014). This model predicts that the nebula will be seen by CTA, and it would reach H.E.S.S. sensitivity if the FIR energy density reaches 2 eV cm^{-3} . We obtain a magnetic field of $21 \mu\text{G}$ with an injection intrinsic break of $\gamma_b = 10^5$ ($\sim 51 \text{ GeV}$), with a low (high) energy index of 1.5 (2.55). These parameters differ from the ones obtained for G54.1+0.3 in Torres et al. (2014) ($B = 14 \mu\text{G}$, $\gamma_b = 5 \times 10^5$, $\alpha_l=1.2$, $\alpha_h=2.8$). With this model, the difference in the magnetic fraction, the energy densities of the IC target photon fields and the age of the system explain why we observe G54.1+0.3 and not G292.0+1.8, even when both are particle dominated.

The radio and X-ray data are also compatible with a high- η model for G292.0+1.8 (see Fig. 5) with $\eta = 0.77$ and a resulting magnetic field of $81 \mu\text{G}$ (similar to the Crab Nebula). The injection in this case has an energy break of $\gamma_b = 2.5 \times 10^5$ ($\sim 130 \text{ GeV}$) and the high energy spectral index changes slightly (2.5). In this case, G292.0+1.8 would not be detected even with CTA also explaining the difference with G54.1+0.3. A deep TeV observation will distinguish between these two models. According to the first model (with $\eta = 0.05$), the TeV flux would be only a factor ~ 2 lower than the H.E.S.S. sensitivity limit in 50 h exposure time.

5 CONCLUSIONS

Despite having similar spin-down power, the value of the magnetic field differs from one to another PWN not only because of the value of η ($B \sim \eta^{1/2}$) differs, but also because their size does ($B \sim R_{PWN}^{-3/2}$). Models with high values of η would explain the low efficiency of some PWNe at X-rays and make them undetectable at VHE. However, we here found that models with high magnetic field and fraction can be constructed only for some of the nebulae that are non-detected at TeV, at the price of stretching other parameters. They seem to work worse than particle dominated models in general, and remain viable only for G76.9+1.0 (for which there are significantly less observational constraints) and G310.6–1.6 (pending the scrutiny of deeper TeV observations). These are the specific conclusions:

- We propose a low magnetization model for N157B with an age of 4.6 kyr and a magnetic field of $13 \mu\text{G}$. The size of the nebula is compatible with the one given by Lazendic et al. (2000), the age with the Sedov age of the remnant (Wang & Gotthelf 1998) and the ejected mass with the lower limit given by Chen et al. (2006). A high magnetization model ($\eta > 0.5$) does not agree with the detection of N157B at TeV energies, which would imply FIR and NIR energy densities much higher than the upper limits obtained by Abramowski et al. (2012).

- N158A non-detection seems to happen because of its smaller age (perhaps also because of a lower photon background?) rather than by having a large magnetization. If this is the case, it will certainly be detected with CTA and likely also by the current generation of instruments. Indeed, just the CMB inverse Compton contribution would produce a CTA source. Without taking into account a possible sig-

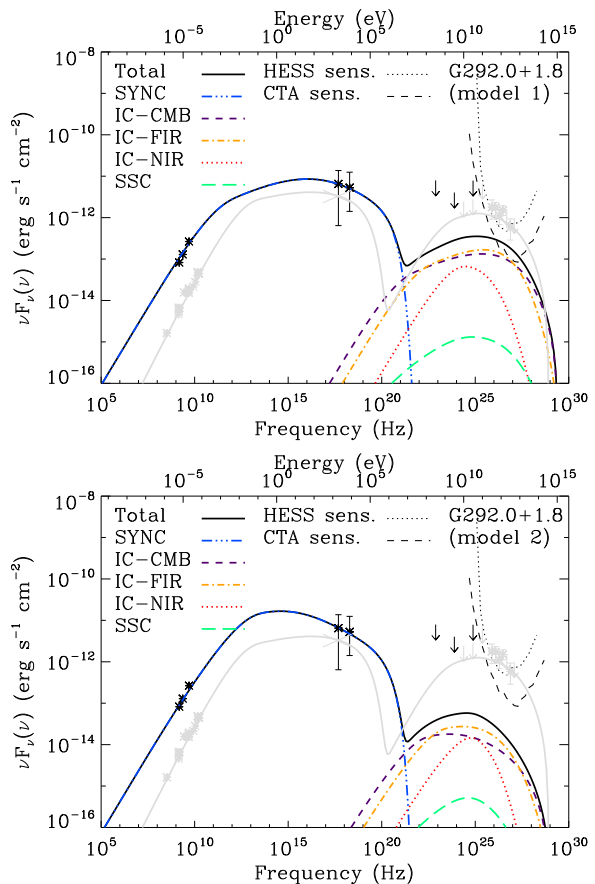


Figure 5. Spectral fits for G292.0+0.18 PWN. In grey, we show the model and data for G54.1+0.3 extracted from Torres et al. (2014).

nificant NIR contribution which would ease the required observation time, we find that if N158A is subject to a FIR energy density of 5 eV cm^{-3} , it can already lead to a detection by H.E.S.S. in 50 hours (lower IC target fields leads to larger integration times, but still within plausible limits). The high- η model(s) explored for N158A has been disregarded as unlikely due to inability to produce a good match to the X-ray data.

- G76.9+1.0 is subject to a large uncertainty given the lack of sufficient observational constraints (only X-ray data are available). This leads to the possibility of accommodating both extremes in the phase space of magnetic fraction. In none of the cases, a TeV detection is expected and it will be difficult to differentiate among models. The FIR and NIR target fields necessary to reach the CTA sensitivity results in more than a factor 100 (1000) in comparison with those obtained by GALPROP for model 1 (2). In such cases, the inverse Compton contribution at X-ray energies would make impossible to fit the spectral slope. Other important parameters as age or the radius of the nebula are not well determined and are needed to make a solid conclusion.

- The low- η models for G310.6–1.6 and G292.0+1.8 predict their detection with H.E.S.S. given sufficient integration time. The CMB inverse Compton contribution reaches the sensitivity curve of a 50 hrs observation in the case

of G310.6–1.6. The magnetic fraction for G292.0+1.8 is one order of magnitude higher than the one obtained for G54.1+0.3 in Torres et al. (2014). This fact and the slight difference in the FIR and NIR energy densities considered in both cases, could explain the lack of detection of G292.0+1.8 at TeV. In both cases, radio and X-ray data are also explained with a high- η model with a magnetic field of 306 μ G for G310.6–1.6 and 81 μ G for G292.0+1.8. However, the high- η model for G310.6–1.6 is not preferred due to its inability to correctly reproduce the spectral break at 6 keV. For G292.0+1.8 instead, a high- η model remains viable and TeV observations would solve the degeneracy.

This work has been done in the framework of the grant AYA2012-39303. Furthermore, A.C.N. and D.F.T. acknowledge the grant PICT Raíces 2012-0605.

References

- Abramowski, A. et al. 2012, *A&A*, 545, L2
 Ackermann M. et al. 2011, *ApJ*, 726, 35
 Arumugasamy, P., Pavlov, G. & Kargaltsev, O. 2013, *XMM-Newton observation of distant, energetic pulsar J2022+3842*, XMM-Newton 2013 Science Workshop
 Arzoumanian, Z., et al. 2008, *ApJ*, 687, 505
 Arzoumanian, Z., Gotthelf, E. V., Ransom, S. M., Safi-Harb, S., Kothes, R. & Landecker, T. L. 2011, *ApJ*, 739, 39
 Campana, R., Mineo, T., De Rosa, A., Massaro, E., Dean, A. J. & Bassani, L., 2008, *MNRAS*, 389, 691
 Caraveo, P. A., Bignami, G. F., Mereghetti, S. & Mombelli, M. 1992, *ApJ*, 395, L103
 Carrigan et al. 2013, arXiv: 1307.4690
 Chaves, R. C. G. et al. 2008, in *AIP Conf. Proc.* 1085, *Proc. 4th International Meeting on High Energy Gamma-ray Astronomy*, ed. F. A. Aharonian, W. Hoffmann & F. Rieger (Melville, NY: AIP), 219
 Chen, Y., Wang, Q. D., Gotthelf, E. V., Jiang, B., Chu, Y. H. & Gruendl, R. 2006, *ApJ*, 651, 237
 Condon, J. J., Griffith, M. R. & Wright, A. E. 1993, *AJ*, 106, 1095
 Duncan, A. R. et al. 1995, *MNRAS*, 277, 36
 Gaensler B. M. & Wallace B. J. 2003, *ApJ*, 594, 326
 Gonzalez, M. E., Kaspi, V. M., Camilo, F., Gaensler, B. M. & Pivovarov, M. J. 2005, *ApJ*, 630, 489
 Gotthelf, E. V. & Wang, Q. D. 2000, *ApJ*, 532, L117
 Griffith, M. R. & Wright, A. E., 1993, *AJ*, 105, 1666
 Heger, A., Fryer, C. L., Woosley, S. E., Langer, N. & Hartmann, D. H. 2003, *ApJ*, 591, 288
 Hughes J. P. et al. 2001, *ApJ*, 559, L153
 Hughes J. P. et al. 2003, *ApJ*, 591, L139
 Hughes J. P. & Friedman R. 2004, *Young Neutron Stars and Their Environments*, IAU Symposium, Vol. 218
 Indebetouw, R. et al. 2009, *ApJ*, 694, 84
 Kaaret, R. et al. 2001, *ApJ*, 546, 1159
 Keek, S., Kuiper, L. & Hermsen, W., 2006, *ATel*, 810.
 Khélifi, B. et al. 2008, in *Proc. 30th ICRC (Mérida)* 2, 803
 Kirshner, R. P., Morse, J. A., Winkler, P. F. & Blair, W. P. 1989, *ApJ*, 342, 260
 Landecker, T. L., Higgs, L. A. & Wendker, H. J. 1993, *A&A*, 276, 522
 Lazendic, J. S., Dickel, J. R., Haynes, R. F., Jones, P. A. & White, G. L. 2000, *ApJ*, 540, 808
 Livingstone, M. A., Kaspi, V. M. & Gavriil, F. P., 2005, *ApJ*, 633, 1095
 Malizia, A. et al. 2007, *ApJ*, 668, 81
 Manchester, R. N., Mar, D. P., Lyne, A. G., Kaspi, V. M. & Johnston, S. 1993, *ApJ*, 403, L29
 Manchester, R. N., Staveley-Smith, L. & Kesteven, M. J. 1993, *ApJ*, 411, 756
 Manchester, R. N., Hobbs, G. B., Teoh, A. & Hobbs, M. 2005, *AJ*, 129, 1993
 Martin, J., Torres, D. F. & Rea, N. 2012, *MNRAS*, 427, 415
 Micelotta, E. R., Brandl, B. R. & Israel, F. P. 2009, *ApJ*, 540, 808
 Mignani, R. P., De Luca, A., Hummel, W., Zajczyk, A., Rudak, B., Kanbach, G. & Słowikowska, A. 2012, *A&A*, 544, A100
 Murphy, T. et al., 2007, *MNRAS*, 382, 382
 Pacini, F. & Salvati, M. 1973, *ApJ*, 186, 249
 Porter, T. A., Moskalenko, I. V. & Strong, A. W. 2006, *ApJ*, 648, L29
 Renaud, M. et al., 2010, *ApJ*, 716, 670
 Reynolds, S. P. 1985, *ApJ*, 291, 152
 Seward, F. D., Harnden, F. R. & Helfand, D. J., 1984, *ApJ*, 287, L19.
 Słowikowska, A., Kandach, G., Borkowski, J. & Becker, W. 2007, *Proc. of the 363 WE-Heraeus Seminar on: Neutron Stars and Pulsars*, eds. W. Becker, H. H. Huang, MPE Report 291, 44
 Tanaka, S. J. & Takahara, F. 2011, *ApJ*, 741, 40
 Tanaka, S. J. & Takahara, F. 2013, *MNRAS*, 429, 2945
 Taylor, J. H. & Cordes, J. M. 1993, *ApJ*, 411, 674
 Tomsick, J. A. et al., 2009, *ApJ*, 701, 811
 Torres, D. F., Martin, J., de Oña Wilhelmi & Cillis, A. 2013, *MNRAS* 436, 3112
 Torres, D. F., Cillis, A., & Martin, J., 2013b, *ApJ Letters*, 763, 4
 Torres, D. F., Cillis, A., Martin, J. & de Oña Wilhelmi, E., 2014, *JHEAp*, 1, 31
 van der Swaluw, E., Achterberg, A., Gallant, Y. A. & Tóth, G. 2001, *A&A*, 380, 309
 van der Swaluw, E. 2004, *Adv. Space Res.*, 33, 475
 Wang, Q. D. & Gotthelf, E. V. 1998, *A&A*, 494, 623
 Wang, Q. D., Gotthelf, E. V., Chu, Y. H., & Dickel, J. R. 2001, *ApJ*, 559, 275
 Williams, B. J. et al. 2008, *ApJ*, 687, 1054
 Winkler P. F. et al. 2009, *ApJ*, 692, 1489
 Zharikov S. V. et al. 2008, *A&A*, 492, 805
 Zharikov S. V. et al. 2013, *A&A*, 554, A120

Table 1. Fixed or assumed model parameters.

| Magnitude | Crab Nebula | N157B | N158A [†] | G76.9+1.0 [‡] | G310.6-1.6 | G292.0+1.8 |
|-------------------------------------|------------------------|------------------------|------------------------|------------------------|------------------------|------------------------|
| Pulsar magnitudes | | | | | | |
| P (ms) | 33.40 | 16.12 | 50.50 | 48 | 31.18 | 135.48 |
| \dot{P} (s s ⁻¹) | 4.21×10^{-13} | 5.18×10^{-14} | 4.79×10^{-13} | 8.64×10^{-14} | 3.89×10^{-14} | 7.53×10^{-13} |
| τ_c (yr) | 1260 | 4936 | 1670 | 8970 | 12709 | 2854 |
| t_{age} (yr) | 940 | 4600 | 760 | 5000 | 1100 | 2500 |
| $L(t_{age})$ (erg s ⁻¹) | 4.5×10^{38} | 4.9×10^{38} | 1.5×10^{38} | 2.96×10^{37} | 5.1×10^{37} | 1.2×10^{37} |
| n | 2.51 | 3 | 2.08 | 3 | 3 | 3 |
| τ_0 (yr) | 730 | 336 | 2340 | 3970 | 11609 | 354 |
| d (kpc) | 2 | 48 | 49 | 10 | 7 | 6 |
| R_{PWN} (pc) | 2 | 10.6 | 0.7 | 4.7 | 1.3 | 3.5 |
| Photon environment | | | | | | |
| $T_{FIR}^{(1)}$ (K) | 70 | 80 | 80 | 25 | 25 | 25 |
| $T_{FIR}^{(2)}$ (K) | - | 88 | - | - | - | - |
| T_{NIR} (K) | 5000 | - | - | 3200 | 3300 | 2800 |
| Injection parameters | | | | | | |
| γ_{min} | 1 | 1 | 1 | 1 | 1 | 1 |

Table 2. Fitted or deduced model parameters.

| Magnitude | Crab Nebula | N157B | N158A [†] | G76.9+1.0 [‡] | G310.6–1.6 | G292.0+1.8 |
|--|----------------------|----------------------|----------------------|------------------------|----------------------|----------------------|
| Pulsar magnitudes | | | | | | |
| L_0 (erg s ⁻¹) | 3.1×10^{39} | 1.1×10^{41} | 3.3×10^{38} | 1.5×10^{38} | 6.1×10^{37} | 7.8×10^{38} |
| M_{ej} (M _⊙) | 9.5 | 20 | 25 | 20 | 9 | 9 |
| Photon environment | | | | | | |
| $w_{FIR}^{(1)}$ (eV cm ⁻³) | 0.4 | 0.7 | 5 (0.2) | 0.13 | 0.62 | 0.42 |
| $w_{FIR}^{(2)}$ (eV cm ⁻³) | - | 0.3 | - | - | - | - |
| w_{NIR} (eV cm ⁻³) | 1 | - | - | 0.33 | 1.62 | 0.70 |
| Injection parameters | | | | | | |
| $\gamma_{max}(t_{age})$ | 7.6×10^9 | 3.8×10^8 | 9.8×10^8 | 5.7×10^8 | 5.7×10^8 | 2.4×10^9 |
| γ_b | 7×10^5 | 10^6 | 3×10^7 | 10^3 | 2×10^6 | 10^5 |
| α_l | 1.5 | 1.5 | 1.8 | 1.5 | 1.5 | 1.5 |
| α_h | 2.5 | 2.75 | 2.6 | 2.7 | 2.5 | 2.55 |
| ϵ | 0.25 | 0.02 | 0.3 | 0.25 | 0.3 | 0.3 |
| Magnetic field | | | | | | |
| $B(t_{age})(\mu G)$ | 82 | 13 | 32 | 3.5 | 8.2 | 21 |
| η | 0.02 | 0.006 | 0.0007 | 0.0017 | 0.0007 | 0.05 |

Some alternative models are commented in the text.

[†]The FIR energy density in the table is the one required for the PWN to be detected by H.E.S.S. (CTA) in 50 hours.

[‡]These parameters correspond to model 1 in Fig. 3, other models are described in the text.